Contents lists available at ScienceDirect

Journal of Molecular Liquids

journal homepage: www.elsevier.com/locate/molliq

Insights on the water effect on deep eutectic solvents properties and structuring: The archetypical case of choline chloride + ethylene glycol

Sara Rozas [a], Cristina Benito [a], Rafael Alcalde [a], Mert Atilhan [b,*], Santiago Aparicio [a,*]

[a] Department of Chemistry, University of Burgos, 09001 Burgos, Spain
[b] Department of Chemical and Paper Engineering, Western Michigan University, Kalamazoo, MI 49008-5462, USA

A B S T R A C T

The effect of water on the properties and nanostructuring of the prototypical choline chloride: ethylene glycol deep eutectic solvent is studied using a combined experimental and theoretical approach. The reported results showed large hydrophilic character of the solvent, which is based on the ability of water molecules to be hydrogen bonded to the different components of the eutectic in a efficient way. The effect of water on the studied fluid is largely dependent on the concentration range but the properties of the eutectic solvent can be maintained up to reasonably large water content. Therefore, the water content in these solvents may be used for tuning and controlling their properties but maintaining properties and features.

1. Introduction

Deep Eutectic Solvents (DESs) are a novel kind of fluids that have gained particular attention in the last few years as an alternative to traditional organic solvents used in the industry [1], but also as an improvement of the closely related materials which are Ionic Liquids (IL) [2,3,7]. Biodegradability [4], low (close to null) volatility [5], low preparation costs [6] and low or non-existent toxicity [7] stand out as their main features, drawing special attention from several researchers [4,8,9]. Likewise, the possibility of developing DES from totally natural, renewable sources, leading to the so-called Natural DESs (NADES) [10,11]. From the structural viewpoint, DES are mixtures of two or more components with a melting point lower than either of its components [12]. The classification of DESs is carried out considering the two types of compounds that are mixed to form the eutectic mixture, thus leading to five different categories [13]. Types I, II, and IV are formed with metallic compounds [14]. The recently proposed Type V DESs involve the combination of molecular compounds [15]. Type III DESs are produced by the combination of two counterpart compounds, namely hydrogen bond acceptors (HBA, usually a salt) and hydrogen bond donors (HBD) [16,17]. A large number of Type III DESs groups are developed by the suitable selection of HBA : HBD combinations as well as from the consideration of HBA:HBD mole ratios. Most of the literature considers Type III DESs for a plethora of possible technological applications [16]. The decrease of melting point upon HBA:HBD mixing for type III DESs stands on the strong hydrogen bond interactions developed formed between HBD and HBA and the charge delocalization [18], which lead to a depression of the lattice energy of the system [19].

The technological applications of DESs consider many different areas, from pharmacological field for drug delivery [20,21] or pharmaceutical formulation [22,23], as extraction solvent in industry [24,25], for gas separation processes or gas sweetening [26,27], synthesis [28,29] and catalysis [30], agri-food sector [31] or polymers [32], among others. Likewise, DESs can be considered as task-specific [33] materials as their properties can be selected and fine-tuned for each considered application through the selection of proper HBA:HBD combinations considering different molecules and mole ratios [34].

Physicochemical [35,36] and microstructural [33,37] properties of DESs have mainly been investigated in the last few years, especially in type III DESs, considering a plethora of HBA:HBD combinations [16]. DESs can also be classified in two large groups: i) hydrophobic [38] and ii) hydrophilic [39]. In the particular case of hydrophilic DESs the behavior of aqueous DESs solutions has been considered [40]. Water in DESs can be considered as an impurity [40]; otherwise, water could be intentionally added to tailor

---

* Corresponding authors.
  E-mail addresses: mert.atilhan@wmich.edu (M. Atilhan), sapar@ubu.es (S. Aparicio).

the physicochemical properties of the DESs [41]. It has been proved that water has a large effect both on the structuring and intermolecular forces of DESs [42,43] as well as in their physicochemical properties [44,45]. Water has been proposed for fine-tuning DESs properties; some researchers have proved that adding water to some DESs leads to a significant lowering of the viscosity, which is pivotal for applying of viscous DESs [46], thus producing improvements in processes such as the extraction efficiency [34,47]. For other applications, when water content decreases the DESs performance, e.g. the decrease of CO_2 solubility [48]. In any case, water has a large effect on DES properties and structuring considering that it may act both as hydrogen donor and acceptor, thus competing and disrupting the HBA : HBD hydrogen bonding network in DESs [49]. The available studies have probed that DES – water mixtures structuring is largely dependent on the water content; nevertheless, DESs nanostructuring is maintained up to remarkably large water content (50 wt% [49]) but macroscopic properties suffer dramatical changes even for low water content. A detailed analysis of the DESs structuring upon hydration have probed different concentration ranges [43]: *i*) "water-in-DES" (0 to 30 water wt%), *ii*) "DES-in-water" (30 to 50 water wt%) and *iii*) DESs aqueous electrolyte solutions (larger than 50 water wt%). In all the cases it has been showed that water is strongly associated with DES components through hydrogen bonding [50].

Although the different structural behavior as a function of water content has been studied as well as the variation of the thermophysical properties upon hydration, the structure – property relationships for DES – water mixtures are still not properly understood. Thereby, regarding the water effect in DESs, this work focuses on the study of a prototypical DESs (ethaline, formed by the mixing of choline chloride, ChCl, and ethylene glycol, EG, Fig. 1) and its properties upon hydration in a wide water content range.

Ethaline has reached special attentions among the studied DESs due to its application in multiple fields, such as electrodeposition [51-53], desulfurization [54], food industry [55], and it has also been investigated in water solution [56]. Alizadeh et al. carried out Ab Initio Molecular Dynamics (AIMD) simulations to investigate the microscopic structure of 1:1 and 1:2 ChCl:EG, and 1:2:1 ChCl:EG:water fluids, finding negligible changes on the structure of the DES in presence of water, only minor changes on EG-Ch+ and EG-Cl- interactions [57]. Similar results were also reported by Lapeña et al. for the same systems [58]. Other study carried out by Yadab et al. showed density and excess molar volume variation with temperature and water content of the DES, showing

water accommodation on ethaline H-bonding network [56]. Zhekenov et al. also investigated from a theoretical point of view water (0 to 1 mol fraction of water) in ethaline behavior regarding structural concerns, exhibiting significant changes: at mole fractions of water under 30 %, water molecules showed to be absorbed in the DES H-bonding network with no structural change on DES, while strong water effects were observed with mole fractions of water above 50% dampening intermolecular and intramolecular interactions in DES [43]. These observations are along the same lines as Sapir et al. [43] for different type III DES. Therefore, although theoretical and experimental studies on DES – water mixtures are reported in the literature, the connection between micro and macroscopic properties is still not fully developed, and combined theoretical and experimental studies are still absent. Therefore, this work considers choline ethaline DES as representing type III DESs to study the water effect on their physicochemical properties for the first time from a combined theoretical and experimental point of view. For the theoretical study, the computational methodology combines a detailed Density Functional Theory (DFT) and Molecular Dynamics (MD) simulations to provide a complete nanoscopic characterization of the water effect on ethaline DES properties, particularly for hydrogen bonding and molecular arrangements in the liquid phases. For the experimental study, different representative physicochemical properties were measured. The experimental and theoretical studies were carried in the 0 to 60 water wt % to consider the different mixture regimes and their transitions. Likewise, the properties of ChCl : EG – Air interface were studied using MD simulations to analyze the nanoscopic features controlling water adsorption/absorption from air humidity, which is of immense relevance to show the properties of this DES when exposed to atmospheric conditions. The reported results contribute to understanding the water effect in physicochemical properties and structuring of type III DESs and provide a nanoscopic justification of the tuning of DES properties by hydration maintaining DESs most relevant features.

2. Materials and methods

2.1. Chemicals

The pure chemicals were obtained from commercial sources (Sigma-Aldrich, purity 99%, ChCl, and 99.8 %, EG) and used as received without further purification. Millipore water (18.2 MΩ cm) was used for all the ethaline + water mixtures. Ethaline (ChCl: EG 1 : 2) DES was prepared by considering suitable amounts of
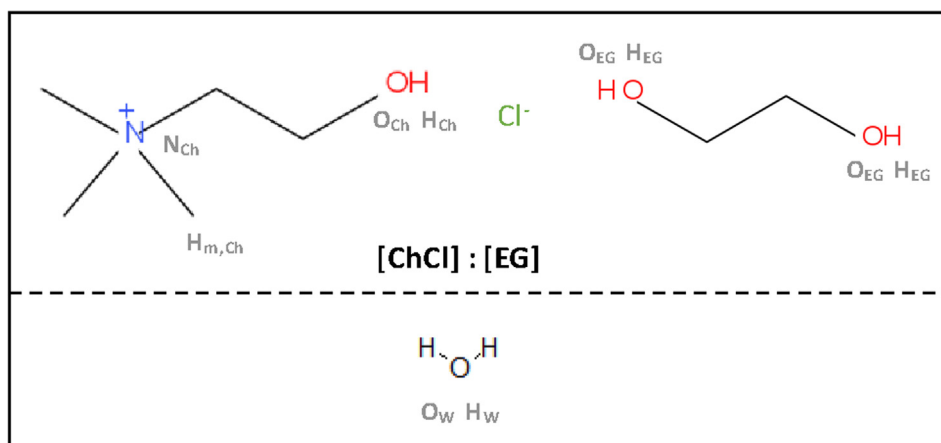

Fig. 1. Molecular structures of compounds used in this work. Atomic labelling used along this work is indicated in grey.

each component by weighing (Mettler AT261 balance, ± 1 10^{-5} g), mixing and heating to 80 °C with stirring at minimum of 300 rpm. A transparent liquid is formed, which remains in liquid state when cooled to room temperature for at least 12 weeks after its preparation. Water content was measured using Karl-Fischer coulometric titration with a Metrohm 831 KF coulometer (±0.3%). Ethaline + water mixtures were prepared in the 0 to 60 wt% (for water content), which corresponds to 0 to 0.96 water mole fraction (Table S1, Supplementary Information).

2.2. Apparatus and procedures

The experimental physicochemical properties (density, shear viscosity, electrical conductivity, thermal conductivity, refractive index and pH) were measured at ambient pressure as a function of temperature. Density (ρ, uncertainty ± 1 10^{-4} g cm^{-3}) was measured using an Anton Paar DMA1001 vibrating tube densimeter, with cell temperature controlled and measured with an internal peltier to ± 0.01 K. Shear viscosity (η, uncertainty ± 2%) was measured using an electromagnetic VINCI Tech EV1000 viscometer, as previously described [59], with the cell temperature controlled by a circulating external bath (Julabo Presto) and measured with platinum resistance thermometer (PRT) to ± 0.01 K. Refractive index was measured with regard to sodium D-line (n_D, uncertainty ± 1 10^{-5}) with a Leica AR600 refractometer with the cell temperature controlled with an external circulator (Julabo F32) and measured with a PRT (±0.01 K). Electrical conductivity (κ, ±0.5% uncertainty) was measured with a VWR pHenomenal conductivity meter, with the cell temperature controlled using a Julabo F32 bath and measured with a PRT (±0.01 K). Thermal conductivity (σ, 5% uncertainty) was measured with a Decagon devices KD2 Thermal analyzer, equipped with a KS-1 sensor (6 cm long, 1.3 mm diameter single needle) with the cell temperature controlled using a Julabo F32 bath and measured with a PRT (±0.01 K). Solvatochromic measurements were carried out using Reichardt's dye indicator (Sigma – Aldrich, 90 % purity). For this purpose, 1 10^{-4} M solutions were prepared and UV–vis spectra were recorded in a LanTechnics UV-18 spectrophotometer (±0.5 nm) with the cell temperature controlled and measured through a peltier system (±0.1 K).

The hydrophilicity of the studied DES was studied by measuring the absorption rates of atmospheric water. These experiments were carried out by placing 15 cm^3 of ethaline in a Petri dish, 90 mm of diameter, with 25.5 cm^2 of liquid surface exposed to air. The water content was measured as a function of time by extracting aliquots (0.01 g) and measuring using a Karl-Fischer coulometer. The atmospheric relative humidity during these experiments was 60 ± 5%. Water absorption kinetic was fitted to the following equation:

$$c_{water} = c_{water}^{\infty}\left(1 - e^{-kt}\right) \qquad (1)$$

Where c_{water} stands for the water content (wt%), c_{water}^{∞} is the limiting absorption value, and k is the kinetic constant.

The properties for neat ethaline obtained in this work are compared with those available in the literature, Table 1. A suitable agreement is inferred for most of the properties with minor divergences justified considering different preparation procedures and water content in the samples. The more significant differences are obtained for dynamic viscosity, for which the preparation procedure, as well as the water content, are known to have large effects.

The physicochemical properties calculated from experimental ones, such as excess or mixing properties, are appropriately defined in the Supplementary Information.

Table 1

Comparison of experimental properties for neat ethaline reporting values obtained in this work and literature values. All values for ChCl : EG (1 : 1) at 298.15 K and atmospheric pressure. Properties: density (ρ), thermal expansion coefficient (α_p), dynamic viscosity (η), electrical conductivity (κ), thermal conductivity (σ), refraction index (n_D) and normalized Reichardt's polarity parameter, E_T^N. For literature data, water content in ppm are reported. (n.r.) stands for non-reported water content.

property	this work	literature
ρ / g cm^{-3}	1.1169	1.11597 (317) [81]
		1.117 (n.r.) [77]
		1.11704 (20) [82]
		1.1174 (50) [83]
		1.11058 (350) [84]
		1.1383 (500) [85]
		1.11646 (790) [86]
		1.11699 (410) [87]
		1.1209 (6462) [88]
$10^3\ \alpha_p$ / K^{-1}	0.500	0.5214 (50) [83]
		0.569 (350) [84]
η / mPa s	28.7	39.60 (317) [81]
		39.96 (n.r.) [77]
		50.6 (6462) [84]
		41 (500) [85]
		48.59 (790) [86]
		47.73 (410) [87]
κ / μS cm^{-1}	7120	8470 (317) [81]
		7120 (n.r.) [77]
		9346 (6462) [84]
σ / W m^{-1} K^{-1}	0.212	0.206 (1000) [89]
n_D	1.4661	1.46889 (317) [81]
		1.46823 (20) [82]
		1.48656 (350) [84]
E_T^N	0.816	0.83 (n.r.) [90]

2.3. Molecular modelling

A detailed molecular modelling DFT analysis was carried out for the ethaline structure and for its interaction with water using ORCA program[60] with B3LYP[61-63] functional, 6–311++G(d,p) basis set and D3[64] dispersion contribution (semiempirical Grimme's method). For neat ethaline, minimal clusters resembling HBA:HBD 1:2 were built and optimized considering the hydrogen bonding sites at ChCl and EG. Likewise, for studying ethaline – water interaction, minimal DES + water clusters (1 DES + 1 water) were built, with water molecules placed around DES components at different possible hydrogen bonding sites, and optimized. Initial structures were built with Avogadro software [65]. After geometrical optimization of the considered molecular clusters, the characterization of the different type interactions was carried out using Quantum Theory of Atoms in Molecule (QTAIM [66]) using MultiWFN software [67]. Intermolecular interactions (hydrogen bonding) are characterized by the formation of several bond critical points (BCPs), along with ring critical points (RCPs) at the center of the interaction region. The strength of hydrogen bonding was quantified using interaction energies, ΔE, which were calculated as the difference between the total energy of the cluster minus formed DES energy and the sum of the corresponding monomers, with Basis Set Superposition Error corrected according to the counterpoise method [64]. The atomic charges were calculated for optimized structures using the ChelpG method [68].

Classical MD simulations to model ethaline + water mixtures were carried out using the MDynaMix v.5.2 [69] package. Simulations were carried out at 303 K and 1 bar, for a 1:2 M ratio composition of ChCl:EG and in the 0 to 60 wt% of water content range. The simulated systems were initially built using Packmol [70] program, considering cubic simulation boxes with the compositions reported in Table S1 (Supplementary Information). The side length of cubic boxes varied from 60 to 82 Å, according to each water percentage. Periodic boundary conditions were applied in the three

directions to simulate infinite system. Additionally, the ChCl – air interface was modelized using the systems described in Table S1 (Supporting Information) with the air described as a mixture of N_2 (72%) + O_2 (23%) + H_2O (5%).The force field parameterizations used for the MD simulations are reported in the Table S2 (Supplementary Information). Force Field parameters for ethaline components (ChCl and EG) were obtained from SwissParam database (Merck Molecular Force Field [71]) with atomic charges obtained from DFT optimized structures for ChCl ionic pair and EG monomer. Water was described using SPC/E [72]. MD simulations were carried out in a two steps approach: *i*) preequilibration step, considering 10 ns long simulations in the NVT (303 K) ensemble at each considered water wt%, with equilibration ensured by constancy of total potential energy and physicochemical properties, and *ii*) 50 ns long simulations in the NPT (303 K and 1 bar). Temperature and pressure were controlled using the Nose-Hoover method [73], with 30 and 1000 ps as temperature and pressure coupling times, respectively. The equations of motion were solved using the Tuckerman-Berne double time step algorithm [74], with long- and short-time steps of 1 and 0.1 fs, respectively. The Ewald summation method [75] was implemented for the Coulombic interactions with cut-off radius of 1.5 nm. Lennard-Jones interactions were treated with 15 Å cut-off distance and Lorentz-Berthelot mixing rules for cross terms.

3. Results and discussion

3.1. Experimental properties

The objective of this study stands on the analysis of the effect of water content on the properties and structure of ethaline DES. Although water may be intentionally added to the DESs for modifying their properties, such as decreasing their viscosity, another relevant source of water adsorption of water stands in contact with atmospheric humidity. The ability of ethaline DES to absorb water from the atmosphere was studied using kinetic experiments of ethaline samples exposed to air at ambient conditions, Fig. 2. The reported values show a 15. 1 wt% of water content upon saturation, which confirms the hydrophilic character of the studied ethaline DES. Nevertheless, the water absorption process shows three stages well-defined mechanism for short (exposures lower than 60 min and saturation at 2.6 wt%), middle (exposures up to 180 min and saturation at 5.3 wt%), and long time (24 h exposure and 15.1 wt% water content) exposures. Therefore, short time exposure of water to atmospheric humidity does not lead to substantial water content; thus, this DES can be handled under con-

trolled conditions without leading to significant water content. The simple kinetic model used to correlate the water absorption is not able to capture these three stages.

The evolution of ethaline density with increasing water content is reported in Fig. 3a (average data after three times measurements for each sample), showing a non-linear evolution but decreasing only a 6.3 wt% on going from pure ethaline to 60 wt% water content at 298.15 K. The reported density values as a function of temperature, Table S3 (Supplementary information) were used to calculate thermal expansion coefficient, α_p, which were obtained from linear fits of density vs. temperature. The reported α_p values, Fig. 3b, show a complex non-linear behavior with maxima around 20 wt% water content. Nevertheless, the evolution of α_p with water content shows three composition regions: *i*) up to roughly 10 wt% with increasing α_p, *ii*) in the 10 – 30 wt% range, with almost constant α_p, and *iii*) water content larger than 30 wt%, for which α_p decreases in a close to linear way. Therefore, these three regions point to different water – ethaline aggregation mechanisms as a function of water content. The experimental density data allowed the calculation of excess molar volume, V^E, Fig. 3c, which is large and negative pointing to large water – ethaline heteroassociation. The minima of V^E appear at roughly 10 wt% water content although the changes in the 10 to 30 wt% are almost negligible, then decreasing (in absolute value) with increasing water content. The large negative V^E for water contents in the 10 to 30 wt% range points to efficient interaction of water molecules with ethaline molecules, with proper fitting of water molecules into ethaline hydrogen bonding networks for developing new hydrogen bonds but maintaining ethaline liquid structuring. This efficient packing leads to positive excess values for α_p, α_p^E, Fig. 3d, i.e. efficient water molecules packing into the ethaline liquid structure, which would justify its hydrophilicity, Fig. 2, as ethaline capacity to fit water molecules into the DES hydrogen bonding network.

The refraction index behavior is reported in Fig. 4a also showing a non-linear evolution with water content especially at lower water content region, which leads to positive mixing refraction index, Δn_D, Fig. 4b, indicating an efficient molecular packing. The three composition regions are also inferred for Δn_D. The calculated molar free volume, f_v [76], show non-linear decrease with increasing water content, with a large decrease on going form neat ethaline to 10 wt% water content, then a smoother decrease up to 30 wt% and then remaining almost constant for larger water content. These results indicate water molecules fitting in ethaline network up to 10 wt%, thus the large decrease in f_v, the increasing size of water-water clusters, with minor changes in ethaline structuring, and then evolving to a water – like fluid for water content larger than 30 wt%.

The studied dynamic properties (η, κ and σ) are reported in Fig. 5. The water content effect on these properties does not clearly show the three regions regime reported for the (non-dynamic) properties reported in Figs. 3 and 4. In the case of viscosity, Fig. 5a, a non-linear evolution is inferred with increasing water content. Although ethaline is a low viscous DES, Table 1, the presence of water molecules decreases remarkably the viscosity of the DES. The evolution of viscosity up to 10 wt% water content show a large decrease (-1.3 mPa s / 1 wt%) followed by a further decrease, with lower slope (-0.4 mPa s / 1 wt%) in the 10 to 30 wt% region, and minor changes (-0.1 mPa s / 1 wt%) for water content larger than 30 wt%. In electrical and thermal conductivity, Fig. 5b and c, a non-linear evolution is also inferred, although the composition regime is not as distinct in Fig. 5c compared to Fig. 5a and b. For the electrical conductivity, Fig. 5b, the increase with water content points to the evolution to electrolyte-like solution behavior upon hydration with increasing presence of charge ionic carriers. Viscosity and electrical conductivity were analyzed together in the so-
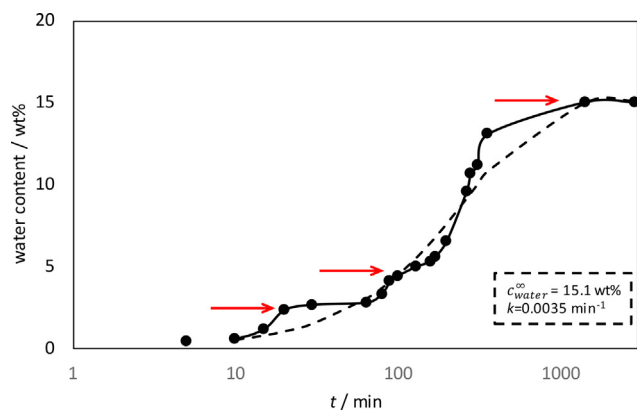

Fig. 2. Kinetics for atmospheric water absorption in ChCl:EG (1:1) at 298 K. Dashed lines show fitting to kinetic model, Eq. (1), with the reported parameters. Red arrows indicate the different stages of the absorption process.
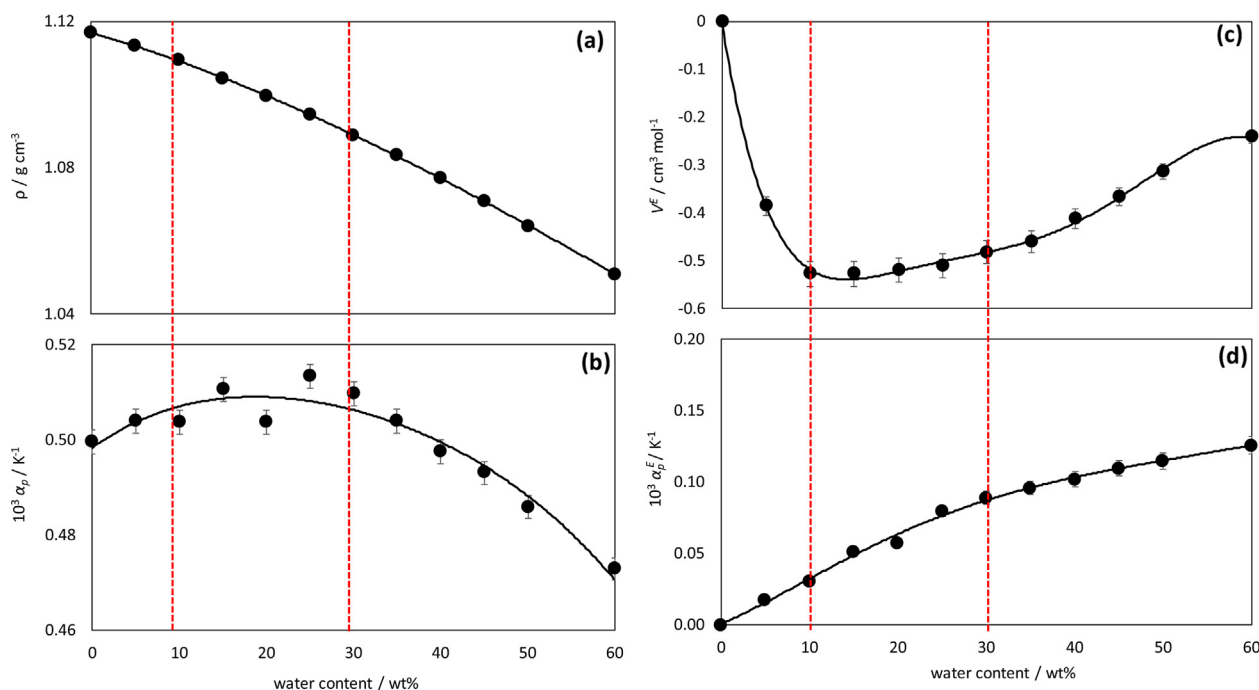
Fig. 3. Experimental (a) density, ρ, (b) thermal expansion coefficient, α_p, (c) excess molar volume, V^E, and (d) excess thermal expansion coefficient, α_p^E, for ChCl:EG (1:1) + water systems as a function of water content at 298.15 K and atmospheric pressure. Continuous lines show polynomial fits to each property. Red dashed lines indicate the different composition regions.

called Walden plot (log–log plot of molar conductivity vs. fluidity), Fig. 6a, which also allow to infer the ionicity as a function of water content [77]. The Walden plot shows a complex non-linear behavior with again the three composition regions showing different trends. As a general trend the increasing water content approaches top the ideal KCl line, i.e. increases the ionic character of the fluids but although the change is inferred in the 0 to 10 wt%, for the 10 to 30 wt% the line remains almost parallel to the reference KCl line, i.e. minor changes in ionic character and for water content larger than 30 wt% it approaches to the reference line. The percentage of ionicity is calculated from the vertical distance to the KCl reference line (ΔW) according to Eq. (2) and reported in Fig. 6b The reported ionicity increases with increases water content as a general trend, as it may be expected from the disrupting effect of water molecules on the HBA – HBA hydrogen bonding leading to the increase of charge carriers (Ch and Cl ions). Nevertheless, although increasing water content from neat ethaline to roughly 10 wt% leads to an increase of ionicity, this increase is very moderate evolving from 17 % in pure ethaline to 23 % for 10 wt% water content. Additional increase up to 30 – 40 wt% water content leads to almost negligible changes in ionicity, even a slight decrease is inferred an only for water content larger than 40 wt% large increase is produced. Therefore, the reported ionicity shows again the three water content regions, which correspond to water interacting with ethaline components than water molecules clustering around HBA – HBD centers, hydration of DES interacting systems, and only for high water content breaking of HBA – HBD interactions leading to an increase of ionicity. It should be remarked that even for 60 wt% water content, the ionicity is only 29 %, which show that HBA – HBD hydrogen bonding is even maintained at significant dilution; thus, isolated HBA – HBD clusters hydrated by surrounding water molecules are expected for large water content with a lower proportion of free ions.

$$\%ionicity = 10^{-\Delta W}100 \tag{2}$$

The temperature evolution of viscosity for each ethaline + water mixture followed a non-Arrhenius behavior and thus it was fitted to Vogel – Fulcher – Tamman (VFT) equation, Eq. (2), with the parameters being reported in Fig. 7. Although the evolution of VFT parameters with water content is complex, the three composition regions may also be inferred from the plots, which confirms that the dynamics of ethaline + water solutions shows different regimes depending on the water content region. In particular, the T_0 parameter, which is related with the glass transition temperature [78] shows non-linear changes with water content, first increasing then remaining almost constant and finally for high water content showing a large decrease. The Angell's fragility parameter, D, may be defined form VFT coefficients according to Eq. (4), where low D values indicate a fragile fluid. The D values for the 0 to 10 wt% water content are 2.2 ± 1.3, which show that ethaline rich solutions are fragile fluids. Literature studies have reported larger values for ethaline D parameter (13.7 and 13.2 from conductivity and relaxation [79]) but we may conclude that ethaline is a fragile liquid. For the 10 to 30 wt% water content, average D is 4.3 ± 0.8, thus decreasing fragility but still being a very fragile fluid, whereas only going to water concentration larger than 40 wt% leads to fragility values larger than 20. Therefore, all the considered ethaline solutions with water content may be considered as fragile liquids although the increasing water content decreases the fragile character, because of the large trend to develop water – ethaline heteroassociations by hydrogen bonding.

$$\eta = Aexp\left(\frac{B}{T - T_0}\right) \tag{3}$$

$$D = \frac{B}{T_0} \tag{4}$$

Another relevant property for a DESs is their polarity, which determines the solubility of relevant solutes for their applications.
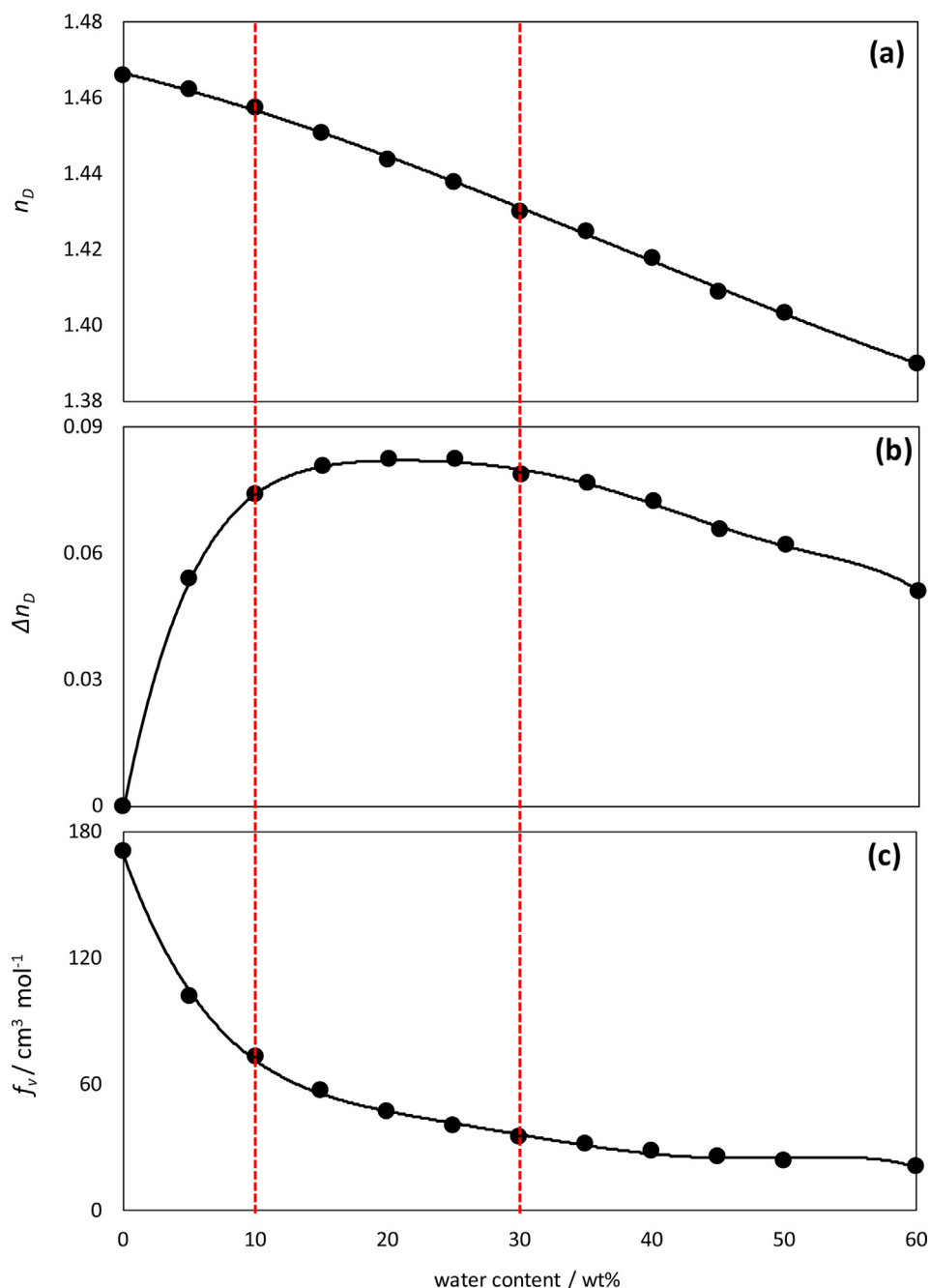
Fig. 4. Experimental (a) refractive index, n_D, (b) mixing refractive index, Δn_D, and (c) molar free volume, f_V, for ChCl:EG (1:1) + water systems as a function of water content at 298.15 K and atmospheric pressure. Red dashed lines indicate the different composition regions.

The polarity as a function of water content was quantified using the E_T^N solvatochromic parameter and the corresponding mixing parameter, ΔE_T^N, Fig. 8. The E_T^N follows a non-linear evolution with increasing water content, Fig. 8a, thus leading to negative ΔE_T^N, Fig. 8b, i.e. lower polarity than expected from a simple dilution process, which can be attributed to the water hydrogen bonding with the ethaline components. The behavior of ΔE_T^N resembles the three composition regions as well as the other physicochemical properties, a large decrease on going up to water 10 wt% then almost constant up to 30 wt% and then decreasing, which justifies the relationship between fluids' polarity and the mechanism(s) of water – DES interactions.

3.2. Molecular modelling: DFT

The experimental properties reported and discussed in the previous section showed a complex mechanism of ethaline hydration with increasing water content which depends on the way of water molecules hydrogen bonding with ethaline components. Therefore, to gain a deeper insight into the developed interactions (hydrogen bonding), DFT studies on the water – ethaline hydrogen bonding were carried out analyzing the different possible interaction sites. It should be remarked that these DFT studies were carried out considering minimal clusters, i.e. 1 : 1 ethaline : water clusters, because of computational restrictions, but they provide information on the developed interactions. Fig. 9 provide the most relevant
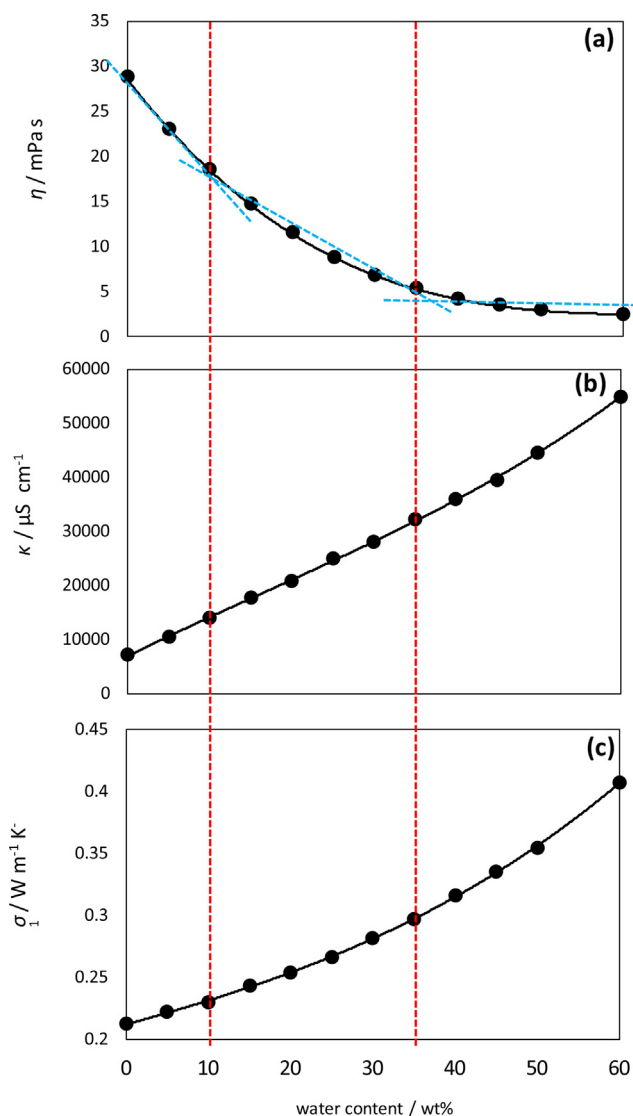
Fig. 5. Experimental (a) dynamic viscosity, η, (b) electrical conductivity, κ, and (c) thermal conductivity, σ, for ChCl:EG (1:1) + water systems as a function of water content at 298.15 K and atmospheric pressure. Red dashed lines indicate the different composition regions.
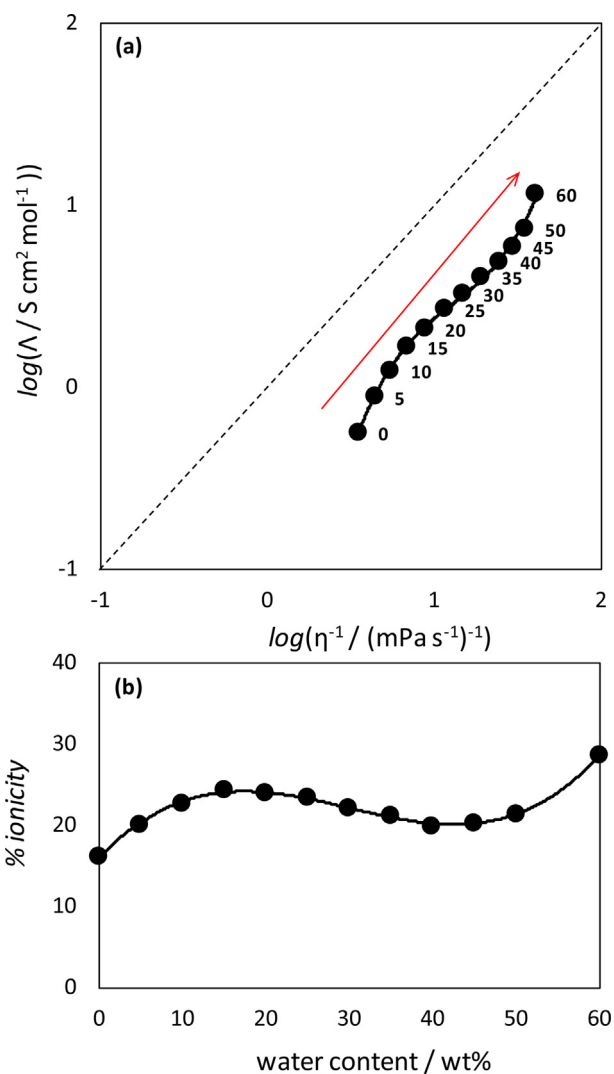

Fig. 6. (a) Walden plot showing log–log plot of molar conductivity, Λ, vs. fluidity, η⁻¹ (where η stands for dynamic viscosity), and (b) calculated percentage of ionicity, for ChCl:EG (1:1) + water systems as a function of water content at 298.15 K and atmospheric pressure. Red arrow in panel a shows increasing water content as indicated with the corresponding point labels (water wt%).

DFT results. Results in Fig. 9 show two different configurations: *i*) A and AW clusters considers Ch and Cl ions interaction via N atom in the cation, and *ii*) B and BW clusters considers anion cation interactions via the OH group in the cation.

The mechanism of ethaline formation was initially analyzed, in absence of water. Ethaline is formed by the combination of EG as HBD interacting with the chlorine anion, with this anion also interacting with the Ch cation. The Cl – Ch interaction may be developed in two different mechanisms: i) Cl – N site in the cation (considering the positive charge of the N center) or ii) Cl – OH site (considering the development of hydrogen bonding). Results in Fig. 9 show stronger interaction when anion – cation interaction is developed through the Ch hydroxyl site (Fig. 9, panel B). Nevertheless, large interaction energy is also inferred for the interaction through N site (Fig. 9, panel A). The Cl - EG distances shows almost negligible differences independently of the considered Ch – Cl mechanism of interaction, and thus point to Cl – EG hydrogen bonding. The QTAIM analysis of these Cl – EG interactions shows the formation of bond paths as well as BCPs whose electronic density, ρ_e, and the corresponding Laplacian, $\nabla^2 \rho_e$, are also included in

Fig. 9. According to the Popelier criteria [80], an intermolecular interaction may be classified as hydrogen bonding when the ρ_e and $\nabla^2 \rho_e$ for the corresponding BCPs are in the 0.002 to 0.04 a.u. and 0.020 to 0.139 a.u ranges, respectively, with larger values indicating stronger hydrogen bonds. Values reported in Fig. 9 for Cl – EG interactions show ρ_e and $\nabla^2 \rho_e$ in the middle of these ranges, thus indicating moderately strong hydrogen bonds. It should be remarked that the formation of the reported DES through the reported Cl – EG hydrogen bonding also leads to EG – EG interactions, which may be classified also as hydrogen bonds according to the developed BCPs. These additional EG – EG interactions also contribute to the large interaction energy upon ethaline formation, as well as to the eutectic stabilization for 1 : 2 ChCl : EG molar ratio.

The case of ethaline - water clusters is also reported in Fig. 9, for DES formed by Ch – Cl interaction through N site (*AW_i*) and for Ch – Cl interaction through OH (*BW_i*). In general *AW_i* leads to lower interaction energies with water molecules when compared with *BW_i*, but water molecules interact efficiently with ethaline components in both cases. Water molecules may inter-
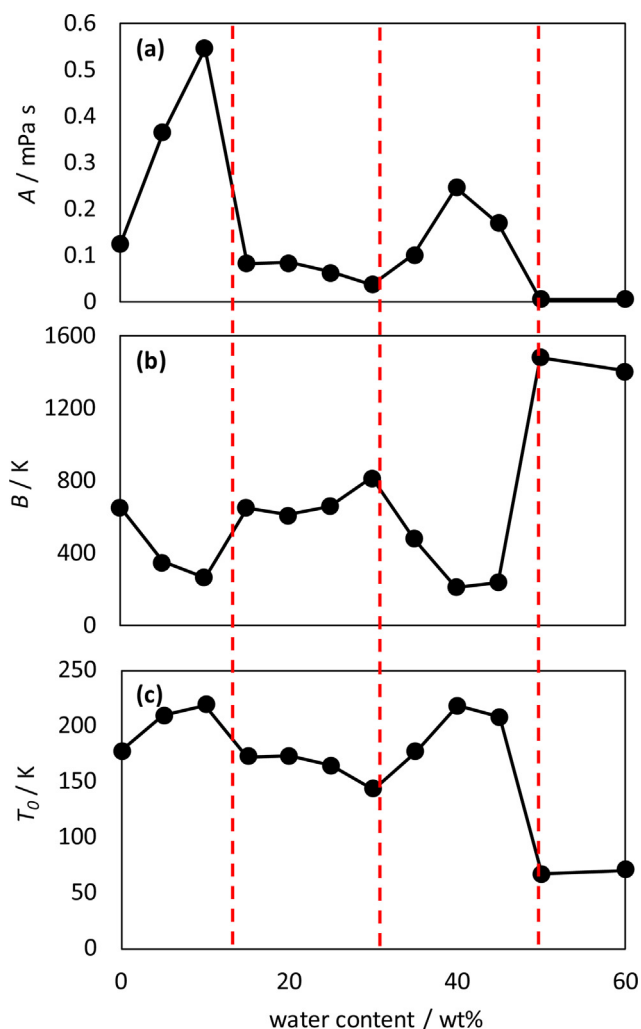
Fig. 7. Fitting coefficients for experimental dynamic viscosity data to Vogel – Fulcher – Tamman equation (Eq. (2)) for ChCl:EG (1:1) + water systems as a function of water content in the experimental temperature range (293.15 to 358.15 K), at atmospheric pressure. Red dashed lines indicated composition regions with different behavior.

Fig. 8. (a) Normalized Reichardt's polarity parameter, E_T^N, and (b) the corresponding mixing parameter, ΔE_T^N, as a function of water content at 298.15 K and atmospheric pressure. In panel a, the dashed line correspond to a an hypothetical linear evolution as a reference.

3.3. Molecular modelling: MD

The reported DFT results provide a characterization of water – ethaline hydrogen bonding but additional effects present in liquid state are missed because of the considered size of the studied clusters. Further characterization of the systems may be inferred from classical MD simulations. The validation of the considered MD approach, i.e. force field parameterization reported in Table S2 (Supplementary Information) is done through the comparison of predicted liquid density and comparison with experimental results (Figure S1, Supplementary Information). The reported predicted density data are overestimating the experimental values but differences in the 0.5 to 1 % are inferred in the full composition range as well as the trend with water content is properly reproduced by MD, thus the considered model may be considered as suitable for describing the water – ethaline systems.

In a first step of the analysis, Radial Distribution Functions (RDFs) for relevant interaction sites were calculated to confirm the mechanism(s) of aggregation. Considering the possible hydrogen bond donor and acceptor sites, the first peak of each RDF was considered, and these peaks were characterized calculating the interatomic (donor – acceptor) distance and the peak intensity. All the selected RDF peaks (i.e. possible donor – acceptor sites and interactions) were systematically arranged in a matrix, named connection matrix, in which interactions are assigned a color code according to the RDF peak height and distance. Hence, the most relevant interactions can be visualized and classified, Fig. 10. All the possible interactions involving N and OH sites in Ch, OH sites in EG, Cl and O sites in water are considered for possible crossed hydrogen bonding. No interactions are inferred through the N site in Ch so Ch interacts through OH sites. The OH site in Ch develop hydrogen bonding both through homoassociation with neighbor

act with available hydrogen bonding sites in the Ch cation (available OH group), with Cl anion, or with the EG sites (OH groups). The differences in terms of interaction energy for the different available sites in the ethaline cluster are very minor, and thus water molecules may interact very efficiently with all these sites. Likewise, the development of interactions with water molecules does not disrupt the ChCl – EG hydrogen bonding, i.e. the DES may fit the available water molecules by additional hydrogen bonding without disrupting their proper interactions. The QTAIM analysis of water – ethaline hydrogen bonds show ρ_e and $\nabla^2 \rho_e$ in the middle to top of the range for hydrogen bonding thus confirming the development of strong hydrogen bonds with water molecules maintaining the most relevant internal features of the DES. The highest $\nabla^2 \rho$ value for AW case was observed at AW_4 with 1.47×10^{-1} a.u.; whereas the highest $\nabla^2 \rho$ value for ABW case was observed at BW_7 with 1.34×10^{-1} a.u. indicating slightly higher bonding capability is established with the DES formed with Ch – Cl interactions through N site. These results confirm that ethaline structuring may be maintained in a large composition range in presence of water as reported in the previous section from experimental results.
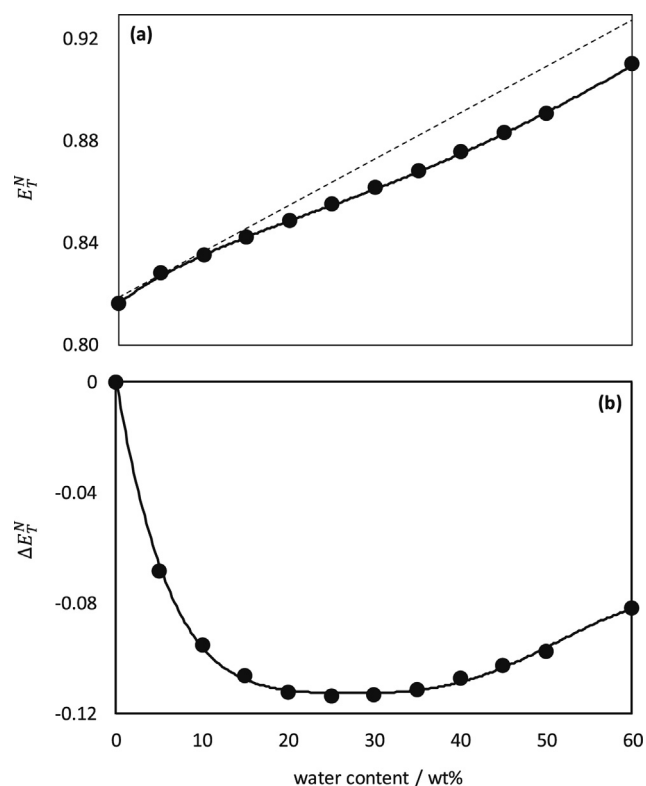
Fig. 9. Results of DFT study of ChCl : EG clusters and ChCl : EG + water clusters for different interaction sites. Counterpoise corrected binding energy, ΔE , and properties for topological critical points obtained from QTAIM analysis (ρ, $\nabla^2\rho$) are reported for relevant sites.

Ch molecules and also heteroassociations with EG, Cl and water molecules in the whole composition range. The main effect with increasing water content stand on the weakening of RDFs for Ch – Ch and Ch – Cl, which points to a decrease of the ethaline cluster sizes as well as for the increase of free cations, in agreement with experimental results (i.e. increase in experimental ionicity). In the case of EG, self-association as well as EG – Ch and EG – Cl are maintained in the whole composition range, only decreasing in intensity with increasing water content. Regarding water molecules they are self-associated as well as interacting with Ch, EG and Cl in the whole composition range.

Additional details on RDFs are reported in Fig. 11. Results in the first row of Fig. 11 (panels a to e) show interacting pairs involving ethaline components. Narrow and strong first RDFs peaks are inferred for all the possible interacting peaks at roughly 2 Å, indicating hydrogen bonding for Ch – Cl, Cl – EG, Ch – Ch and EG – EG. The position of these peaks does not change with increasing water content, only then intensity decreases. In the case of water – ethaline RDFs, Fig. 11 (panels f to h), water is hydrogen bonded to all the available sites in the DES as confirmed by the first intense peak in the corresponding RDFs. Water may act both as hydrogen bond

donor or acceptor both for Ch (Fig. 11, panels f and f') or EG (Fig. 11, panels g and g'). The self-association of water is confirmed in Fig. 11i in the whole composition range. The integration of RDFs reported in Fig. 12 for the first peak, i.e. molecules prone to develop hydrogen bonding, allows to calculate the solvation numbers, N, for each site, i.e. the number of molecules involved in each interaction for a certain interaction site, Fig. 12. The general evolution of N with increasing water content is non-linear for all the possible interaction sites. Regarding Ns corresponding to self-association of ethaline, the main feature corresponding to Cl – EG interaction decreases steeply up to 10 – 15 wt% of water and then in a smoother way; nevertheless, even for high water content, Cl – EG remains. Similar behavior is inferred for Cl – Ch interactions, which probes that the DES remains hydrogen bonded in the whole composition range, decreasing the size of the cluster. For the association of water with ethaline components, the most significant interaction is developed through Cl – water contacts, with a lower number of interactions with Ch and EG hydroxyl sites with the water molecules acting as hydrogen bond donors. It should be remarked that with increasing water content, the number of interacting pairs of water with Ch and EG with water molecules acting
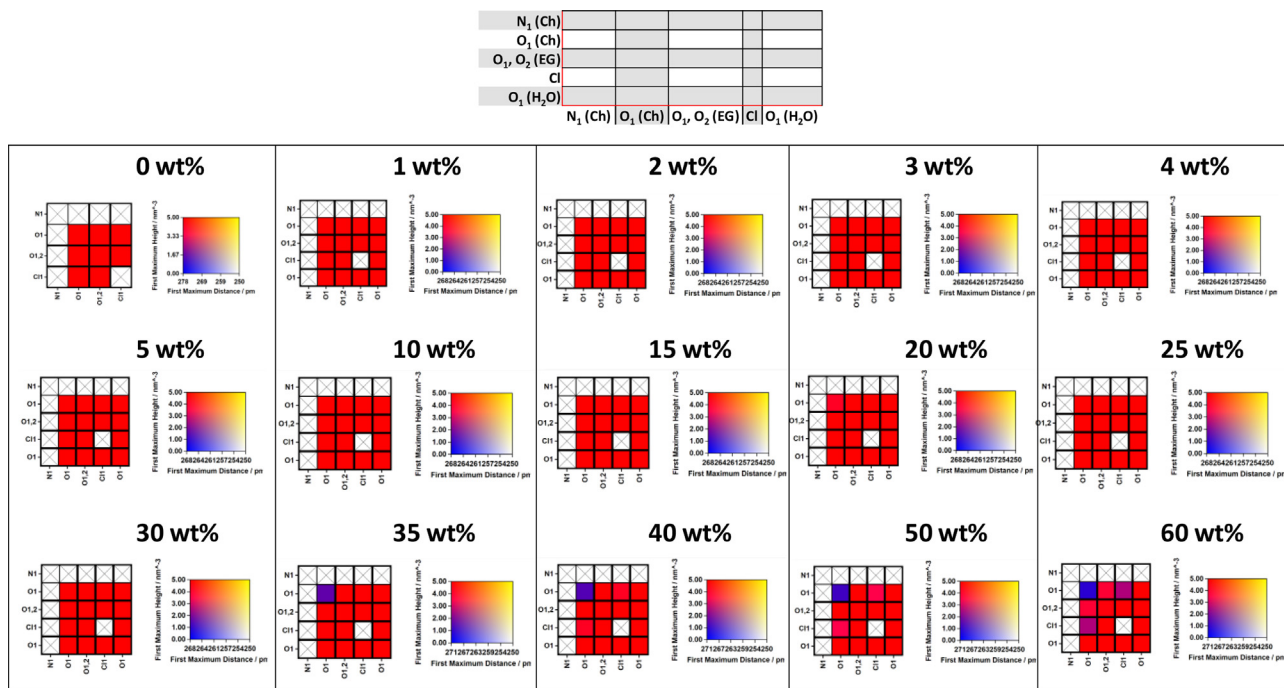
Fig. 10. Connection matrix analysis of interactions in ChCl : EG (1 :2) + water from MD simulations at 303 K. Water content is indicated as wt%. The atomic elements included in the matrix are reported in the table on the top. The color in each square represents both the intensity and distance of the first maximum in the corresponding RDF (for color scale, see the right-hand side).

as donors increases. In contrast, those for water molecules acting as acceptor decreases, which point to water molecules increasingly involved in water – water interactions, with the increasing occupation of water oxygen sites, thus only allowing the interaction with the ethaline OH sites through the H atoms in water. Water self-association increasing with increasing water constant is also confirmed in Fig. 12.

The particular distribution around each type of molecule in ethaline – water systems is analyzed through Spatial Distribution Functions (SDFs), as reported in Fig. 13. The distribution around

Ch shows a highly localized distribution around the OH site, with EG and water competing in the same region. Nevertheless, in the 10 to 30 water wt% the distribution is slightly different to that in up to 5 wt% range. Likewise, for large water content (greater than30 wt%), then distribution around the central Ch changes with EG molecules occupying all the regions around the Ch. Thus, EG molecules are shifted by the presence of water molecules competing for the Ch hydroxyl site. Considering central EG molecules, a similar behavior to that around Ch is inferred and around central water molecules. Therefore, the competing effect of water mole-
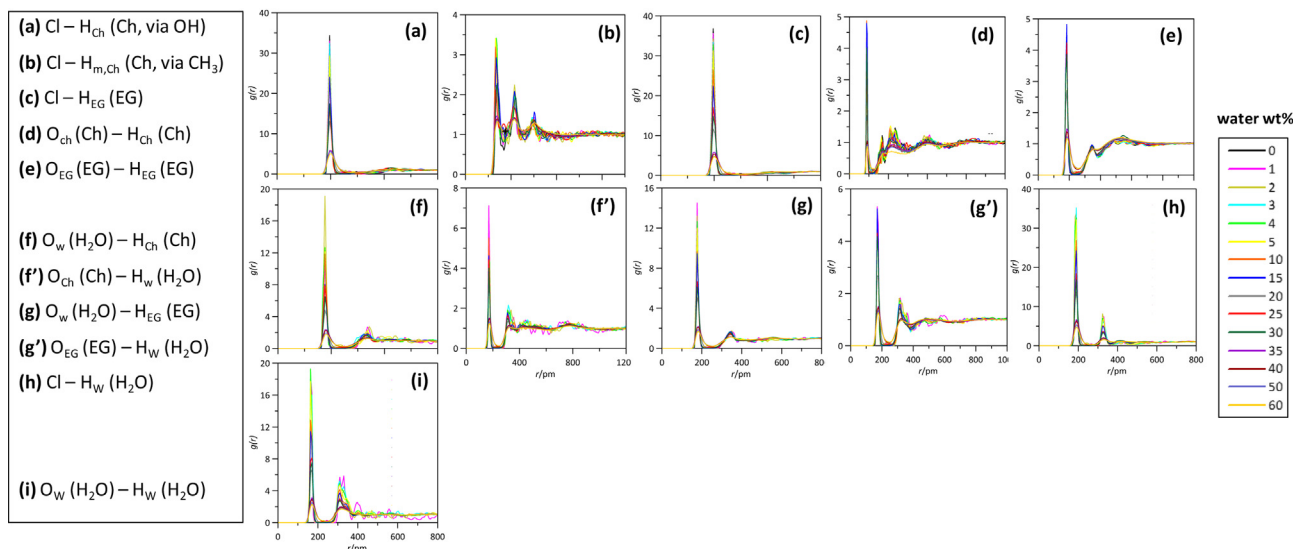
Fig. 11. Site – site radial distribution functions, $g(r)$, for the reported interacting pairs (atom labelling as in Fig. 1) in ChCl : EG (1 :2) + water from MD simulations at 303 K. Water content is indicated as wt%.
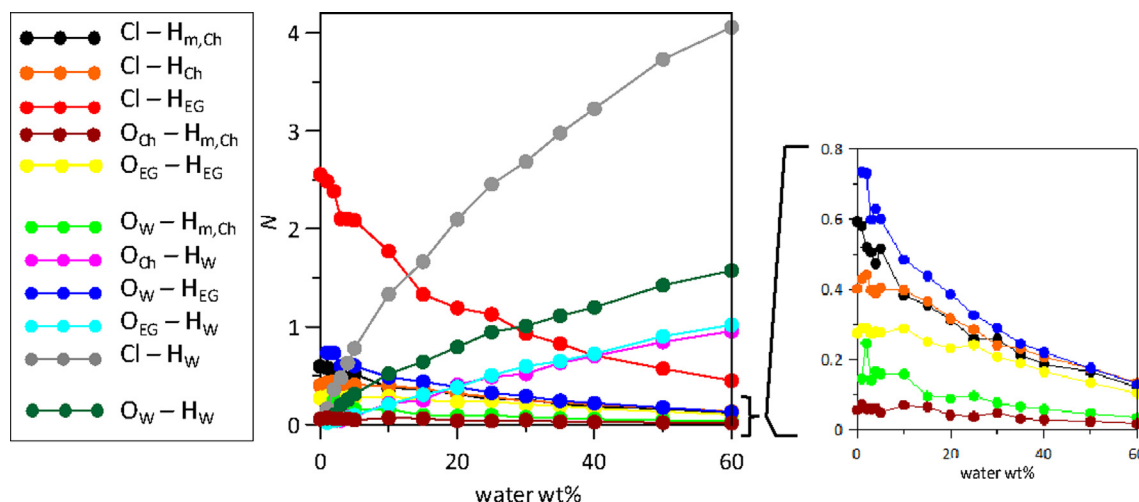
Fig. 12. Solvation numbers, N, obtained from the integration of radial distribution functions reported in Fig. 11, corresponding to the first solvation sphere, defined as the first minimum in the corresponding radial distribution function in ChCl : EG (1 :2) + water from MD simulations at 303 K. Water content is indicated as wt%.
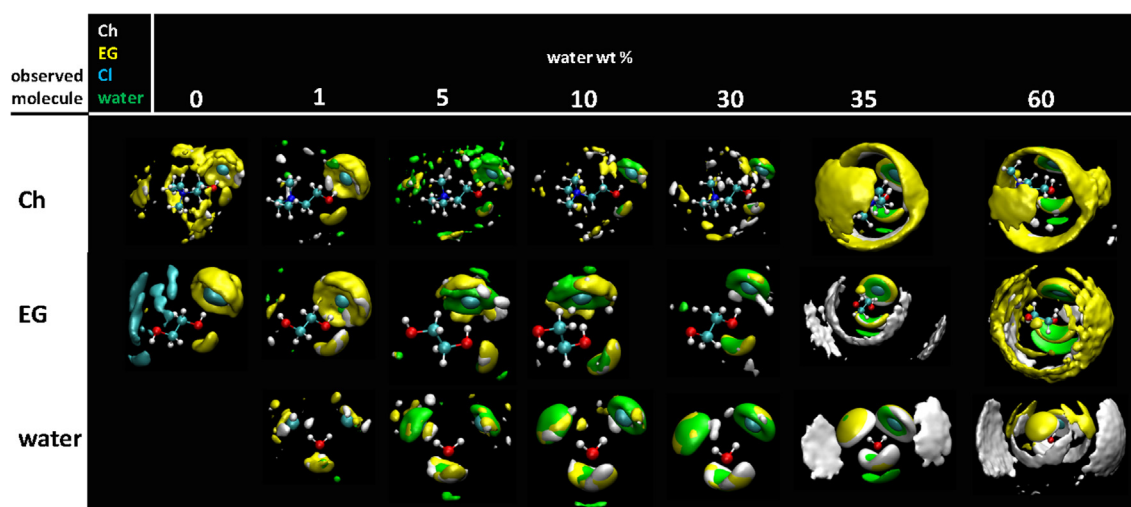

Fig. 13. Spatial distribution functions around central molecules in ChCl : EG (1 :2) + water from MD simulations at 303 K. Water content is indicated as wt%.

cules for the available hydrogen bonding sites follows the three composition regions as the experimental properties.

The developed intermolecular forces are quantified through the intermolecular interaction energies, E_{int}, Fig. 14. The stronger forces are produced from Ch – Cl interactions, considering its electrostatic nature, which decrease upon increasing water content because of the development of water – Cl hydrogen bonding. The remaining interactions between ethaline components also decrease with increasing water content because of the increase of interactions with water, thus decreasing the size of the aggregates and the corresponding E_{int}. Nevertheless, the extension of hydrogen bonding was quantified using a geometrical criterion considering 3.5 Å and 60° for donor – acceptor separation and orientation, Fig. 15. A large number of interacting pairs develop hydrogen bonds decreasing or increasing their number with increasing water content. The solvation of Cl anions by hydrogen bonding with water molecules appears as the main factor in the mixture structuring, which is paired with the decrease of Cl – EG interactions. It should be remarked the sudden change (decrease) in hydrogen bonding for some pairs at water 30 wt%, which may be produced by the spatial rearrangement inferred from SDFs in Fig. 13, therefore confirming the fluids' restructuring for composition above water 30 wt%.

The decrease of self-association between ethaline component with increasing water content is confirmed although hydrogen bonding remains even for high water content, in agreement with ionicity results reported in Fig. 6.

The reported theoretical results have probed the large hydrophilicity of the studied DES, with large effects on DES properties and nanoscopic structuring, as well as the possibility of capturing water from atmospheric humidity. MD simulations of ethaline – air (described as a mixture of N_2, O_2, and water) interface were carried out to characterize the absorption of water molecules from the air at the nanoscopic scale. The structure of the ethaline – air interface is reported in Fig. 16a. An adsorbed layer composed of external N_2 molecules, followed by O_2 molecules and then of water molecules contact with ethaline is rapidly formed (<1 ns). Water molecules cross the interface from this adsorbed layer and are absorbed into the liquid ethaline, whereas N_2 and O_2 molecules remain adsorbed at the interface. This effect is quantified through the density profiles in the direction perpendicular to the interface reported in Fig. 16 b. Likewise, the corresponding interaction energies upon adsorption / absorption are reported in Fig. 17 confirming the strong water – ethaline interactions (specially with Cl anions) in contrast with the weaker interactions of ethaline with N_2 and O_2, in spite of
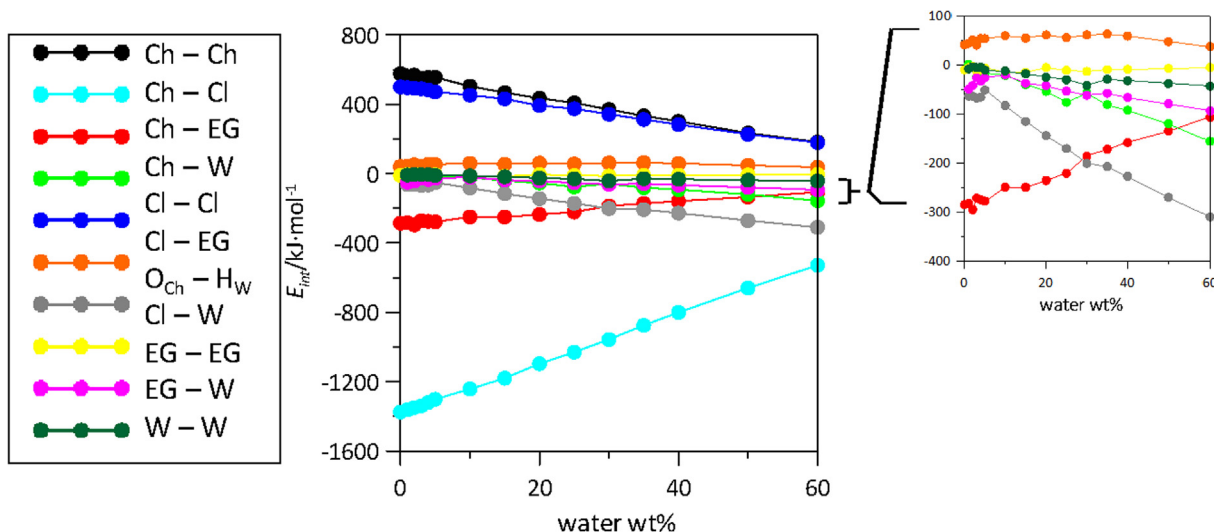
Fig. 14. Intermolecular interaction energy, E_{int} (sum of Lennard-Jones and coulombic contributions), for the reported interacting pairs in ChCl : EG (1 :2) + water from MD simulations at 303 K. Water content is indicated as wt%.
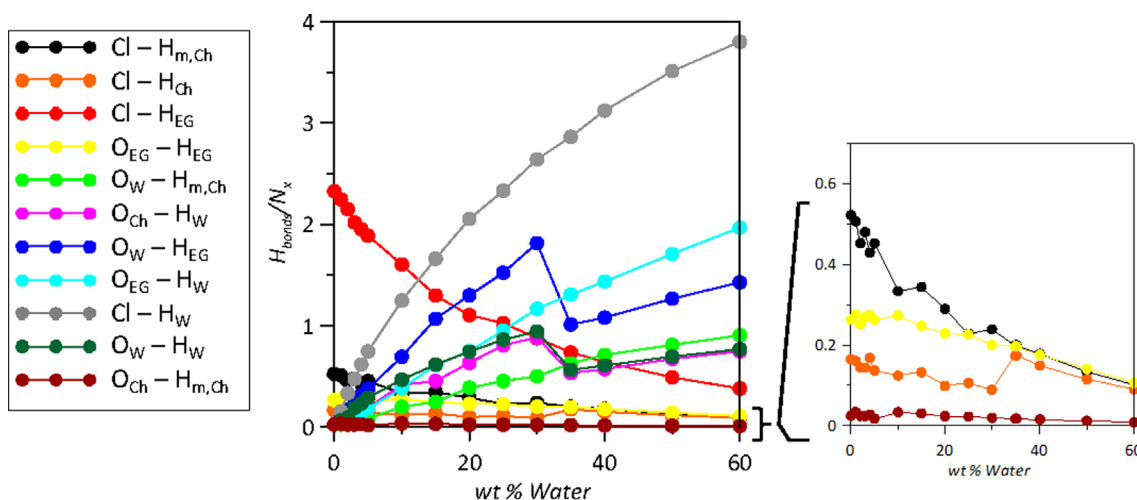

Fig. 15. Number of hydrogen bonds per molecule, H_{bonds}/N, for the reported interacting pairs in ChCl : EG (1 :2) + water from MD simulations at 303 K. Water content is indicated as wt%.
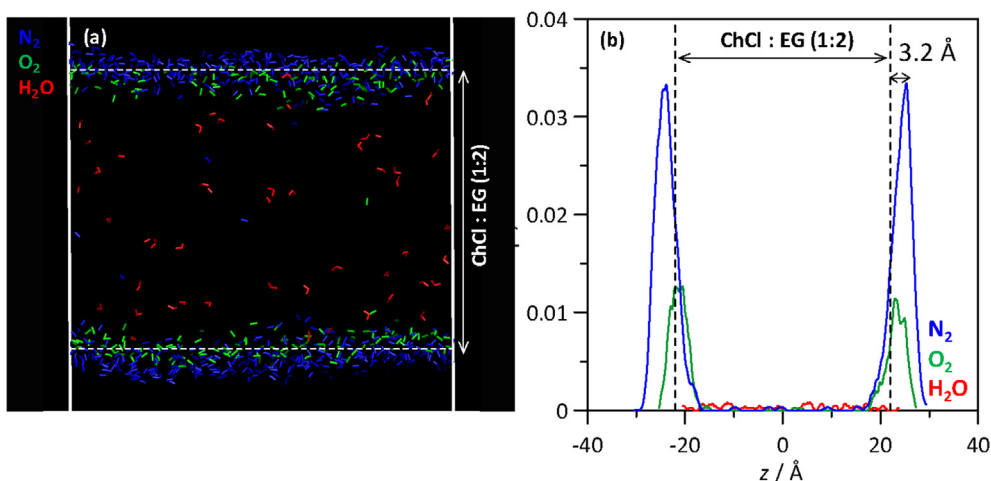

Fig. 16. (a) Snapshot of gas molecules distribution at the ChCl : EG (1 :2) - air ($N_2 + O_2$ + water) interface and (b) and (b) the corresponding density profiles in the direction perpendicular to the interface from MD simulations at 303 K.
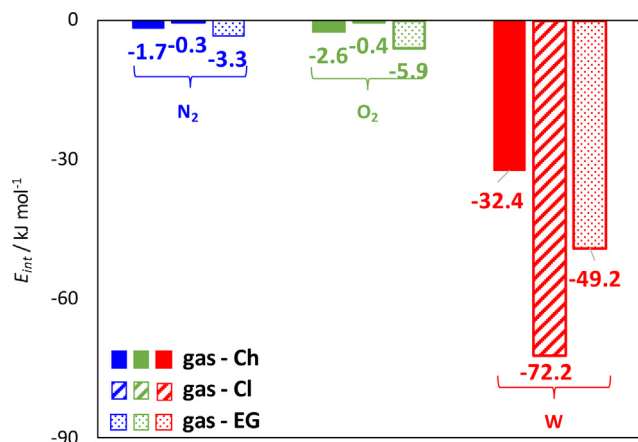
Fig. 17. Interaction energies, E_{int}, for gas molecules at the ChCl : EG (1 :2) - air (N_2 + O_2 + water) interface from MD simulations at 303 K.

the developed adsorbed layer at the interface. Therefore, the reported interfacial results confirm that water molecules are able to be adsorbed at the ethaline interface then crossing the boundary evolving to the liquid phase in a short time (a few ns), which would result in quick adsorption rates, specially for the initial stages of water sorption as inferred from results in Fig. 2.

4. Conclusions

The structural and physicochemical properties of ethaline Deep Eutectic Solvent function as a function of the degree of hydration studied in this work. The reported experimental and theoretical studies show water molecules changing ethaline properties through the development of hydrogen bonding, thus competing with the proper self-association of ethaline components. Nevertheless, the evolution of the properties and structuring does not follow a linear behavior with water content, three different regions are inferred: i) up to 10 wt% (characterized by minimal perturbations of the ethaline properties and structuring), ii) 10 to 30 wt% (characterized by increasing water self-aggregation but maintaining the main features of the eutectic although decreasing the size of ethaline aggregates), and iii) water content greater than 30 wt%, in which water self-aggregation prevails and ethaline small clusters are dispersed into a water solvent, and thus although hydrogen bonding between the ethaline components is mainly maintained, the most relevant features of the eutectic are lost. Therefore, ethaline may be hydrated up to roughly 30 wt% maintaining most of the features of the eutectic, and thus considering that exposition to atmospheric humidity does not lead to water contents larger than 15 wt%, this eutectic can be handled at open-air which leads to a reasonable degree of hydration but maintaining the most relevant fluid properties. The controlled exposure of hydrophilic deep eutectics, such as ethaline, may be used to obtain a reasonable degree of hydration, which may be used to control, fine-tune and optimize relevant physicochemical properties such as viscosity, but to maintain the most relevant structural properties of the studied fluids.

Declaration of Competing Interest

The authors declare that they have no known competing financial interests or personal relationships that could have appeared to influence the work reported in this paper.

Appendix A. Supplementary data

Supplementary data to this article can be found online at https://doi.org/10.1016/j.molliq.2021.117717.

References

[1] S.C. Cunha, J.O. Fernandes, Extraction techniques with deep eutectic solvents, TrAC 105 (2018) 225–239.
[2] S. Sarmad, J.-P. Mikkola, X. Ji, Carbon dioxide capture with ionic liquids and deep eutectic solvents: a new generation of sorbents, Chem. Sus. Chem. 10 (2) (2017) 324–352.
[3] S.K. Singh, A.W. Savoy, Ionic liquids synthesis and applications: An overview, J. Mol. Liq. 297 (2020) 112038, https://doi.org/10.1016/j.molliq.2019.112038.
[4] L.I.N. Tomé, V. Baião, W. da Silva, C.M.A. Brett, Deep eutectic solvents for the production and application of new materials, Appl. Mater. Today 10 (2018) 30–50.
[5] Q. Zhang, K.D.O. Vigier, S. Royer, F. Jérôme, Deep eutectic solvents: syntheses, properties and applications, Chem. Soc. Rev. 41 (2012) 7108–7146.
[6] F. del monte, D. Carriazo, M.C. Serrano, M.C. Gutiérrez, M.L. Ferrer, Deep eutectic solvents in polymerizations: a greener alternative to conventional syntheses, Chem. Sus. Chem. 7 (2014) 999–1009.
[7] X. Ge, C. Gu, X. Wang, J. Tu, Deep eutectic solvents (DESs)-derived advanced functional materials for energy and environmental applications: challenges, opportunities, and future vision, J. Mater. Chem. A 5 (2017) 8209–8229.
[8] S.C. Cunha, J.O. Fernándes, Extraction techniques with deep eutectic solvents, TrAC 105 (2018) 225–239.
[9] A. Shishov, A. Bulatov, M. Locatelli, S. Carradori, V. Andruch, Application of deep eutectic solvents in analytical chemistry. A review, Microchem. J. 135 (2017) 33–38.
[10] Y. Liu, B. Friesen, J.B. McAlpine, D.C. Lankin, S.N. Chen, G.F. Pauli, Natural deep eutectic solvents: properties, applications, and perspectives, J. Nat. Prod. 81 (2018) 679–690.
[11] H. Vanda, Y. Dai, W.G. Wilson, R. verpoorte, Y.H. Choi, Green solvents from ionic liquids and deep eutectic solvents to natural deep eutectic solvents, Compt. Ren. Chim. 21 (6) (2018) 628–638.
[12] G. García, S. Aparicio, R. Ullah, M. atilhan, Deep eutectic solvents: physicochemical properties and gas separation applications, Energy Fuels 29 (2015) 2616–2644.
[13] S. Dutta, K. Nath, Prospect of ionic liquids and deep eutectic solvents as new generation draw solution in forward osmosis process, J. Water Process Eng. 21 (2018) 163–176.
[14] E.L. Smith, A.P. Abbott, K.S. Ryder, Deep eutectic solvents (DESs) and their applications, Chem. Rev. 114 (2014) 11060–11082.
[15] D.O. Abranches, M.A.R. Martins, L.P. Silva, N. Schaeffer, S.P. Pinho, J.A.P. Coutinho, Phenolic hydrogen bond donors in the formation of non-ionic deep eutectic solvents: the quest for type V DES, Chem. Comm. 55 (2019) 10253–10256.
[16] B.B. Hansen, S. Spittle, B. Chen, D. Poe, Y. Zhang, J.M. Klein, A. Horton, L. Adhikari, T. Zelovich, B.W. Doherty, B. Gurkan, E.J. Maginn, A. Ragauskas, M. Dadmun, T.A. Zawodzinski, G.A. Baker, M.E. Tuckerman, R.F. Savinell, J.R. Sangoro, Deep eutectic solvents: a review of fundamentals and applications, Chem. Rev. 121 (3) (2021) 1232–1285.
[17] F.M. Perna, P. Vitale, V. Capriati, Deep eutectic and their applications as green solvents, Curr. Opin. Green Sustain. Chem. 21 (2020) 27–33.
[18] D.V. Wagle, L. Adhikari, G.A. Baker, Computational perspectives on structure, dynamics, gas sorption, and bio-interactions in deep eutectic solvents, Fluid Phase Equilibr. 448 (2017) 50–58.
[19] T. Aissaoui, I.M. AlNashef, U.A. Qureshi, Y. Benguerba, Potential applications of deep eutectic solvents in natural gas sweetening for CO_2 capture, Rev. Chem. Eng. 33 (6) (2017) 523–550.
[20] M.H. Zainal-Abidin, M. Hayyan, G.C. Ngoh, W.F. Wong, C.Y. Looi, Emerging frontiers of Deep eutectic solvents in drug Discovery and drug delivery systems, J. Control. Release 316 (2019) 168–195.
[21] S.N. Pedro, M.G. Freire, C.S.R. Freire, A.J.D. Silvestre, Deep eutectic solvents comprising active pharmaceutical ingredients in the development of drug delivery systems, Expert Opinion on Drug Delivery 16 (5) (2019) 497–506.
[22] S. Emami, A. Shayanfar, Deep eutectic solvents for pharmaceutical formulation and drug delivery applications, Pharm. Dev. Technol. 25 (7) (2020) 779–796.
[23] H. Palmelund, M.P. Andersson, C.J. Asgreen, B.J. Boyd, J. Rantanen, K. Löbmann, Tailor-made solvents for pharmaceutical use? Experimental and computational approach for determining solubility in deep eutectic solvents (DES), Int. J. Pharm. 1 (2019) 100034.

[24] Y. Dai, G.-J. Witkamp, R. Verpoorte, Y.H. Choi, Natural deep eutectic solvents as a new extraction media for phenolic metabolites in Carthamus tinctorius L, Anal. Chem. 85 (13) (2013) 6272–6278.

[25] V.M. Paradiso, A. Clemente, C. Summo, A. Pasqualone, F. Caponio, Towards green analysis of virgin olive oil phenolic compounds: Extraction by a natural deep eutectic solvent and direct spectrophotometric detection, Food Chem. 212 (2016) 43–47.

[26] M. Atilhan, S. Aparicio, Review and perspectives for effective solutions to grand challenges of energy and fuels technologies via novel deep eutectic solvents, Energy Fuels 35 (8) (2021) 6402–6419.

[27] M. Atilhan, S. Aparicio, Review on chemical enhanced oil recovery: Utilization f ionic liquids and deep eutectic solvents, J. Petrol. Sci. Eng. 205 (2021) 108746.

[28] H. Qin, X. Hu, J. Wang, H. Cheng, L. Chen, Z. Qi, Overview of acidic deep eutectic solvents on synthesis, properties and applications, Green Energy & Enviroment 5 (1) (2020) 8–21.

[29] J.D. Mota-Morales, R.J. Sánchez-Leija, A. Carranza, J.A. Pojman, F. del Monte, G. Luna-Bárcenas, Free-radical polymerizations of and in deep eutectic solvents: Green synthesis of functional materials, Prog. Polym. Sci. 78 (2018) 139–153.

[30] A.E. Unlu, A. Arikaya, S. Takac, Use of deep eutectic solvents as catalyst: A mini-review, Green Proc. Synth. 8 (2019) 355–372.

[31] A. Misan, J. Nadpal, A. Stupar, M. Pojic, A. Mandic, R. Verpoorte, The perspectives of natural deep eutectic solvents in agri-food sector, Critical Rev. Food Sci. Nutr. 60 (15) (2020) 2564–2592.

[32] A. Roda, A.A. Matias, A. Paiva, A.R.C. Duarte, Polymer Science and Engineering Using Deep Eutectic Solvents, Polymers 11 (2019) 912.

[33] S. Kaur, M. Kumari, H.K. Kashyap, Microstructure of Deep Eutectic Solvents: Current Understanding and Challenges, J. Phys. Chem. B 124 (2020) 10601–10616.

[34] Y. Dai, G.J. Witkamp, R. Verpoorte, Y.H. Choi, Tailoring properties of natural deep eutectic solvents with water to facilitate their applications, Food Chem. 187 (2015) 14–19.

[35] X. Xu, J. Range, G. Gygli, J. Pleiss, Analysis of thermophysical properties of deep eutectic solvents by data integration, J. Chem. Eng. Data 65 (3) (2020) 1172–1179.

[36] K. Jafari, M.H. Fatemi, P. Estele, Deep eutectic solvents (DESs): A short overview of the thermophysical properties and current use as base fluid for heat transfer nanofluids, J. Mol. Liq. 321 (2021) 114752.

[37] S. Kaur, A. Gupta, H.K. Kashyap, Nanoscale spatial heterogeneity in deep eutectic solvents, J. Phys. Chem. B 120 (27) (2016) 6712–6720.

[38] D.J.G.P. van Osch, C.H.J.T. Dietz, S.E.E. Warrag, M.C. Kroon, The curious case of hydrophobic deep eutectic solvents: a story on the discovery, design, and applications, ACS Sustainable Chem. 8 (2020) 10591–10612.

[39] Y. Ma, Q. Wang, T. Zhu, Comparison of hydrophilic and hydrophobic deep eutectic solvents for pretreatment determination of sulfonamides from aqueous environments, Anal. Methods 11 (46) (2019) 5901–5909.

[40] C. Ma, A. Laaksonen, C. Liu, X. Lu, X. Ji, The particular effect of water on ionic liquids and deep eutectic solvents, Chem. Soc. Rev. 47 (2018) 8685–8720.

[41] P.E. Valverde, T.A. Green, S. Roy, Effect of water on the electrodeposition of copper from a deep eutectic solvent, J. Appl. Electrochem. 50 (2020) 699.

[42] T. Zhekenov, N. Tolsanbayev, Z. Kazakbayeva, D. Shaha, F.S. Mjalli, Formation of type III deep eutectic solvents and effect of water on their intermolecular interactions, Fluid Phase Equilibr. 441 (2017) 43–48.

[43] L. Sapir, D. Harries, Restructuring a Deep Eutectic Solvent by Water: The nanostructure of hydrated choline chloride/urea, J. Chem Theory Comput. 16 (5) (2020) 3335–3342.

[44] A.Y.M. Al-Murshedi, H.F. Alesary, R. Al-Hadrawi, Thermophysical properties in deep eutectic solvents with/without water, J. Phys.: Conf. Series 1294 (2019) 052041, https://doi.org/10.1088/1742-6596/1294/5/052041.

[45] Y. Wang, C. Ma, C. Liu, X. Lu, X. Feng, X. Ji, Thermodynamic study of choline chloride-based deep eutectic solvents with water and methanol, J. Chem. Eng. Data 65 (5) (2020) 2446–2457.

[46] X.Liu, N. Fu, Q. Zhang, S. Cai, Q. Wang, D. Han, B. Tang, Green tailoring with water of choline chloride deep eutectic solvents for the extraction of polyphenols from palm samples, J. Chromatogr. Sci. 57 (2019) 272-278.

[47] M. Vilková, J. Plotka-Wasylka, V. Andruch, The role of water in deep eutectic solvent-base extraction, J. Mol. Liq. 304 (2020) 112747.

[48] W.C. Su, D.S.H. Wong, M.H. Li, Effect of water on solubility of carbon dioxide in (aminomethanamide + 2-hydroxy-N, N. N-trimethylethanaminium Chloride), J. Chem. Eng. Data 54 (2009) 1951–1955.

[49] O.S. Hammond, D.T. Bowron, K.J. Edler, The effect of water upon deep eutectic solvent nanostructure: an unusual transition from ionic mixture to aqueous solution, Angew. Chem. Ed. 129 (2017) 9914–9917.

[50] P. Kumari, Shobhna, S. Kaur, H.K. Kashyap, Influence of hydration on the structure of reline deep eutectic solvent: a molecular dynamics study, ACS Omega 3 (11) (2018) 15246–15255.

[51] R. Bernasconi, G. Panzeri, G. Firtin, B. Kahyaoglu, L. Nobili, L. Magagnin, Electrodeposition of ZnNi alloys from choline chloride/ethylene glycol deep eutectic solvent and pure ethylene glycol for corrosion protection, J. Phys. Chem. B 124 (47) (2020) 10739–10751.

[52] E. Barrado, S. García, J.A. Rodríguez, Y. Castrillejo, Electrodeposition of indium on W and Cu electrodes in the deep eutectic solvent choline chloride-ethylene glicol (1:2), J. Electroanal. Chem. 823 (2018) 106–120.

[53] W. Li, J. Hao, S. Mu, W. Liu, Electrochemical behavior and electrodeposition of Ni-Co alloy from choline chloride-ethylene glycol deep eutectic solvent, Appl. Surf. Sci. 507 (2020) 144889.

[54] M. Rogošić, K.Z. Kučan, Deep eutectic solvents based on choline chloride and ethylene glycol as media for extractive denitrification/desulfurization/dearomatization of motor fuels, J. Ind. Eng. Chem. 72 (2019) 87–99.

[55] M.E. Alañón, M. Ivanović, A.M. Gómez-Caravaca, D. Arráez-Román, A. Segura-Carretero, Choline chloride derivative-based deep eutectic liquids as novel Green alternative solvents for extraction of phenolic compounds from olive leaf, Arab. J. Chem. 13 (1) (2020) 1685–1701.

[56] A. Yadav, J.R. Kar, M. Verma, S. Naqvi, S. Pandey, Densities of aqueous mixtures of (choline chloride + ethylene glycol) and (choline chloride + malonic acid) deep eutectic solvents in temperature range 283.15–363.15 K, Thermochim. Acta 600 (2015) 95–101.

[57] V. Alizadeh, F. Malberg, A.A.H. Pádua, B. Kirchner, Are there magic compositions in deep eutectic solvents? Effect of composition and water content in choline chloride/ethylene glycol from Ab Initio molecular dynamics, J. Phys. Chem. B 124 (2020) 7433–7443.

[58] D. Lapeña, L. Lomba, M. Artal, C. Lafuente, B. Giner, Thermophysical characterization of the deep eutectic solvent choline chloride:ethylene glicol and one of its mixtures with water, Fluid Phase Equilibr. 492 (2019) 1–9.

[59] R. Alcalde, G. García, M. Atilhan, S. Aparicio, Systematic study on the viscosity of ionic liquids: measurement and prediction, Ind. Eng. Chem. Res. 54 (43) (2015) 10918–10924.

[60] F. Neese, The ORCA program system, WIREs Comput. Mol. Sci. 2 (1) (2012) 73–78.

[61] C. Lee, W. Yang, R.G. Parr, Development of the Colle-Salvetti correlation-energy formula into a functional of the electron density, Phys. Rev. B 37 (1988) 785–789.

[62] A.D. Becke, Density-functional exchange-energy approximation with correct asymptotic behavior, Phys. Rev. A 38 (1988) 3098–3100.

[63] A.D. Becke, Density-functional thermochemistry. III. The role of exact exchange, J. Chem. Phys. 98 (1993) 5648–5652.

[64] S. Simon, M. Duran, J. Dannenberg, How does basis set superposition error change the potential surfaces for hydrogen-bonded dimers?, J Chem. Phys. 105 (1996) 11024.

[65] S. Adams, P. de Castro, P. Echenique, J. Estrada, M.D. Hanwell, P. Murray-Rust, P. Sherwood, J. Thomas, J. Townsend, The Quixote project: collaborative and open quantum chemistry data management in the internet age, J. Chemiformatics 3 (1) (2011), https://doi.org/10.1186/1758-2946-3-38.

[66] R.F.W. Bader. Atoms in Molecules: A Quantum Theory. (1990) (Oxford).

[67] T. Lu, F. Chen, Multiwfn: A multifunctional wavefunction analyzer, J. Comput. Chem. 33 (2012) 580–592.

[68] C.M. Breneman, K.B. Wiberg, Determining atom-centered monopoles from molecular electrostatic potentials. The need for high sampling density in formamide conformational analysis, J. Comput. Chem. 11 (3) (1990) 361–373.

[69] A.P. Lyubartsev, A. Laaksonen, MdynaMix – A scalable portable parallel MD simulation package for arbitrary molecular mixtures, Comput. Phys. Commun. 128 (3) (2000) 565–589.

[70] L. Martínez, R. Andrade, E.G. Birgin, J.M. Martínez, Packmol: A package for building initial configurations for molecular dynamics simulations, J. Comput. Chem. 30 (2009) 2157–2164.

[71] V. Zoete, M.A. Cuendet, A. Grosdidier, O. Michielin, SwissParam: a fast force field generation tool for small organic molecules, J. Comput. Chem. 32 (2011) 2359–2368.

[72] H.J.C. Berendsen, J.R. Grigera, T.P. Straatsma, The missing term in effective pair potentials, J. Phys. Chem. 91 (24) (1987) 6269–6271.

[73] W.G. Hoover, Canonical dynamics: Equilibrium phase-space distributions, Phys. Rev. A 31 (1985) 1695.

[74] M. Tuckerman, B.J. Berne, G.J. Martyna, Reversible multiple time scale molecular dynamics, J. Chem. Phys. 97 (3) (1992) 1990–2001.

[75] U.L. Essmann, M.L. Perera, T. Berkowitz, H. Darden, H. Lee, L.G. Pedersen, A smooth particle mesh ewald method, J. Chem. Phys. 103 (19) (1995) 8577–8593.

[76] A.S.L. Gouveia, L.C. Tome, I.M. Marrucho, Density, viscosity, and refractive index of ionic liquid mixtures containing cyano and amino acid-based anions, J. Chem. Eng. Data 61 (1) (2016) 83–93.

[77] Y. Wang, W. Chen, Q. Zhao, G. Jin, Z. Xue, Y. Wang, T. Mu, Ionicity of deep eutectic solvents by Walden plot and pulsed field gradient nuclear magnetic resonance (PFG-NMR), Phys. Chem. Chem. Phys. 22 (44) (2020) 25760–25768.

[78] C.A. Angell, Formation of glasses from liquids and biopolymers, Science 167 (1995) 1924–1935.

[79] D. Reuter, C. Binder, P. Lunkenheimer, A. Loidl, Ionic conductivity of deep eutectic solvent, Phys. Chem. Chem. Phys. 21 (2019) 6801–6809.

[80] U. Koch, P.L.A. Popelier, Characterization of C-H-O hydrogen bonds on the basis of charge density, J. Phys. Chem. 99 (1995) 9747–9754.

[81] D. Lapeña, L. Lomba, M. Artal, C. Lafuente, B. Giner, Thermophysical characterization of the deep eutectic solvent choline chloride:ethylene glycol and one of its mixtures with water, Fluid Phase Equilibr. 492 (2019) 1–9.

[82] R.B. Leron, A.N. Soriano, M.-H. Li, Densities and refractive indices of the deep eutectic solvents (choline chloride + ethylene glycol or glycerol) and their aqueous mixtures at the temperature ranging from 298.15 to 333.15 K, J. Taiwan Inst. Chem. Eng. 43 (4) (2012) 551–557.

[83] R.B. Leron, M.H. Li, High-pressure volumetric properties of choline chloride–ethylene glycol based deep eutectic solvent and its mixtures with water, Thermochim, Acta 546 (2012) 54–60.

[84] D.Z. Troter, Z.B. Todorovic, D.R. Dokic-Stojanovic, B.S. Dordevic, V.M. Todorovic, S.S. Konstantinovic, V.B. Veljkovic, The physicochemical and

thermodynamic properties of the choline chloride-based deep eutectic solvents, J. Serb. Chem. Soc. 82 (9) (2017) 1039–1052.

[85] F.S. Mjalli, J. Naser, Viscosity model for choline chloride – based deep eutectic solvents, Asia-Pac. J. Chem. Eng. 10 (2) (2015) 273–281.

[86] N.F. Gajardo-Parra, V.P. Cotroneo-Figueroa, P. Arevana, V. Vesovic, R.I. Canales, Viscosity of Choline Chloride-Based Deep Eutectic Solvents: Experiments and Modeling, J. Chem. Eng. Data 65 (11) (2020) 5581–5592.

[87] N.F. Gajardo-Parra, M.J. Lubben, J.M. Winnert, A. Leiva, J.F. Brennecke, R.L. Canales, Physicochemical properties of choline chloride-based deep eutectic solvents and excess properties of their pseudo-binary mixtures with 1-butanol, J. Chem. Themodyn. 133 (2019) 272–284.

[88] R.K. Ibrahim, M. Hayyan, M.A. AlSaadi, S. Ibrahim, A. Hayyan, M.A. Hashim, Physical properties of ethylene glycol-based deep eutectic solvents, J. Mol. Liq. 276 (2019) 794–800.

[89] T.H. Ibrahim, M.A. Sabri, N.A. Jabbar, P. Nancarrow, F.S. Mjalli, I. AlNashef, Thermal Conductivities of Choline Chloride-Based Deep Eutectic Solvents and Their Mixtures with Water: Measurement and Estimation, Molecules 25 (2020) 3816.

[90] M. Aryafard, A. Karimi, A.R. Harifi-Mod, B. Minofar, Molecular Dynamics Simulations, Solvatochromic Parameters, and Preferential Solvation in Aqueous Solutions of Ethaline, Ethylene Glycol, and Choline Chloride, J. Chem. Eng. Data 65 (9) (2020) 4556–4566.